RESEARCH ARTICLE

ADVANCED
MATERIALS
INTERFACES
Open Access

www.advmatinterfaces.de

Photo-Induced Electric Field Effects on Water Droplets Generated in a LiNbO₃ Opto-Microfluidic Platform

Giovanni Bragato, Annamaria Zaltron, Michele Zanardi, Riccardo Zamboni, Maddalena De Ros, and Cinzia Sada*

In this work, droplets elongation as a result of the photo-induced photovoltaic electric field is presented and modeled. Moving water droplets are generated in microfluidics channels by means of a droplet-based opto-microfluidic platform integrated in lithium niobate (LN). A cross-junction is engraved on the substrate as droplets generator, on top of which a z-cut iron-doped lithium niobate (Fe:LN) crystal is placed in order to build up photo-induced electric field as a result of photovoltaic effect promoted upon suitable illumination. Droplets detection is realized by optical waveguides, designed in a Mach-Zehnder Interferometer (MZI) configuration on the same substrate. The dynamics of droplet elongation is investigated, highlighting the impact of the photovoltaic electric field on the droplet dimension and surface tension.

1. Introduction

Recently, the development of new opto-microfluidic sensing devices[1–4] has gained increasing interest due to the promising features allowed by the combination of microfluidic and optical stages on the same platform, that addresses the need for integrating in the same portable device several tools which carry out different tasks, e.g., manipulation of droplets, sensing of refractive index[5] and pH,[6] targets identification and sorting.[7] In particular, the manipulation of droplets in microfluidic systems is a wide and complex field.[8] As it is well-known in literature, droplets can be generated and processed either in closed microfluidics[3,9,10] or in open configuration, the latest being unconstrained from channels-driven fluxes.[11,12] The possibility of exploiting external electric fields to move droplets, sort them,

merge them and modify their shape has been explored in the last years,[11–13] being the actuation and control of liquid droplets a major challenge not only for many industrial processes but also for chemical, biological, and medical applications. Active control of droplets by means of electric fields, both on surfaces and within microchannels, typically requires the deposition of metallic electrodes on the employed substrate or microfluidic chip, which in turn need voltage suppliers, hence limiting the portability of the device and in fact almost excluding reconfigurable features. An interesting alternative to metallic electrodes is provided by light-induced phenomena able to locally modify the conductivity of the substrate, as the case of the photovoltaic effect (PhV). PhV arises typically in crystals with non-centrosymmetric structure[14,15] and is related to photoexcitation and re-combination phenomena that lead to electric charges redistribution and, consequently, space-charge electric field building up. A valid candidate that exhibits photovoltaic effect for this kind of applications is lithium niobate (LN), which has also been proposed recently by our group[3,16,17] for Lab-On-a-Chip systems. This insulating material is well-known in the field of integrated optics due to its interesting electro-optical, non-linear optical, piezoelectric, and photorefractive properties, which have been successfully combined with microfluidic devices.[18–24] The high chemical resistance and biocompatibility[25] of LN, together with its high optical transmission in the range 350–3500 nm and its easy interfaceability with polymers and glasses, represent an added value and qualify this material as an optimal choice for biological, and medical applications. In particular, in the case of LN, the photovoltaic properties can be tuned and significantly enhanced by local doping the material. One of the most common dopant is iron, which enables the introduction of two valence states impurities: Fe^{2+}, acting as a donor, and Fe^{3+}, acting as an acceptor of free charges, respectively. In fact, when a suitable light pattern irradiates an iron-doped lithium niobate (Fe:LN) crystal, electrons in the bright areas are excited from donors (that remain positively charged) to the conduction band and migrate until acceptor's centres are reached in the not illuminated region (becoming negatively charged). The spatial charge distribution so created is responsible for the building up of the space-charge field, that behaves as a virtual reconfigurable microelectrode. The term "virtual" refers to the fact that no metal electrodes need to be deposited to generate an electric field at the surface of this

G. Bragato, A. Zaltron, M. Zanardi, M. De Ros, C. Sada
Physics and Astronomy Department "Galileo Galilei"
University of Padua
Via Marzolo 8, Padova 35131, Italy
E-mail: cinzia.sada@unipd.it
R. Zamboni
Institute of Applied Physics
University of Münster
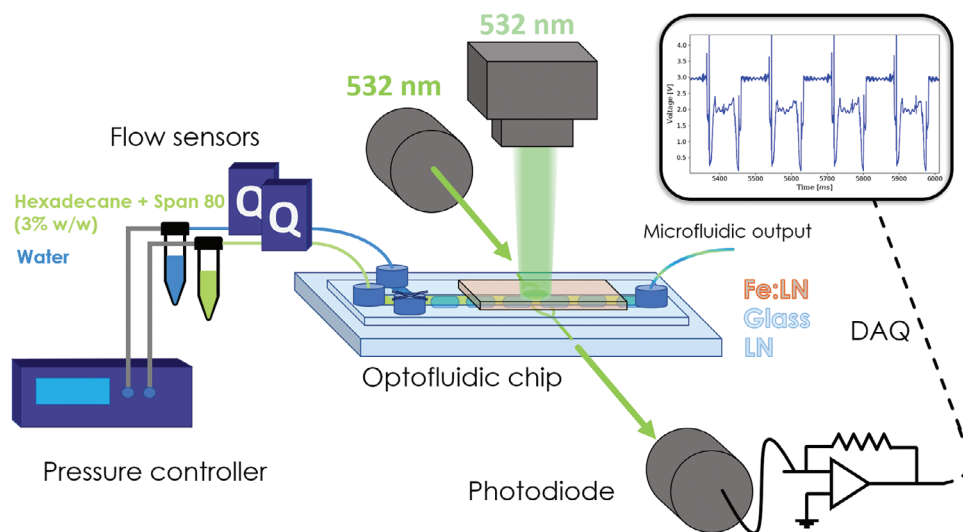Corrensstr. 2/4, 48149 Münster, Germany

Figure 1. Scheme of the opto-microfluidic setup.

insulating material. The possibility to exploit virtual electrodes to modify the droplet dimension is of particular interest in the study of electric field assisted phenomena in micro-reactors chambers with special attention to whispering gallery modes (WGMs) excitation.[26–29] It is well known that in ring resonator WGMs can be formed through total internal reflection provided that the mode path matches the right phase conditions of the propagating field. This requires given ring geometries that can be easier to be achieved by a fine tuning of the ring shape.[30] Droplets are excellent candidates for this kind of applications because it is possible to obtain the desired refractive index contrast by using water/oil systems to get total internal reflection.[31,32] The possibility to modify the droplet shape on demand to match the ring resonator conditions represents a very interesting playground for future applications in biosensing and optical sensing in general. This is especially true if the droplet shape can be tailored with photo-induced effects that therefore are flexible, versatile, and not permanent.

In this work, a new concept of droplet-based opto-microfluidic platform integrated in LN is introduced, combining microfluidics with integrated optics and photovoltaic phenomena to enable in the future the modification and actuation of dispersed objects within water droplets. The opto-microfluidic device consists of a cross-junction engraved on a LN substrate and sealed with a glass slide, while a z-cut Fe:LN crystal placed on the top of the chip is employed to generate light-induced photovoltaic fields, which interact with the droplets. Droplets detection is realized by exploiting optical waveguides, designed to obtain a Mach-Zehnder Interferometer (MZI) configuration. In particular, a novel phenomenon is observed, which results from the interaction of the photo-induced electric field and the water droplets dispersed in hexadecane. Droplets lengths was proven to be sensitive to the photo-induced electric field with a dependence on the droplets velocity and on the dissolved electrolytes concentration. Moreover, the magnitude of this effect can be tuned by modifying the doping level of the employed Fe:LN.

2. Experimental Section

Droplets were generated by exploiting an optofluidic chip:[3] a cross-junction was engraved on a lithium niobate (LN) substrate such that the main channel was perpendicular to an array of Ti-indiffused waveguides realized in a Mach-Zehnder interferometer (MZI) configuration. The waveguides were coupled to laser light, allowing the detection of droplets flowing within the main channel (width $w_c = 200$ μm, height $h_c = 100$ μm) and the measurement of length and velocity of each single droplet. The substrate was sealed with a glass cover (thickness of around 1 mm; a brief discussion on the influence of the glass thickness can be found in the Supporting Information). A detailed description of this optofluidic chip, including design and fabrication, has been provided by the group in Ref. [9].

MilliQ® water was used as dispersed phase (flow rate Q_d) while Hexadecane (Sigma–Aldrich) with 3 % w/w concentration of SPAN® 80 surfactant (Sigma–Aldrich) as continuous phase (flow rate Q_c), hence producing water droplets dispersed in the latter. The surface tension between water and hexadecane with the surfactant concentration employed in this work was measured by the pendant drop method obtaining $\gamma_0 = 4.27 \pm 0.04$ mNm^{-1}. The flow rates were controlled by a pressure pump OB1 MK3 (Elveflow, Paris, France) in feedback with flowmeters BFS Coriolis (Bronkhorst, AK Ruurlo, Holland). Liquids were injected in the chip through microfluidic inlets. A scheme of the opto-microfluidic setup is reported in **Figure 1**.

The cross-junction engraved in the substrate was employed in a T-junction configuration by closing one of the two lateral channels perpendicular to the main channel. In such a geometry, provided that the working regime was the squeezing one,[33] droplets length L is given by:[34,35]

$$L = (\varepsilon + \omega\phi)\, Ca^{-m} \tag{1}$$

where $Ca = \mu_c v/\gamma$ is the capillary number, μ_c is the viscosity of the continuous phase, v is droplets velocity, γ the surface tension

Table 1. List of all the flow rates' combinations in this work. The standard deviation σ_Q associated to each flow rate value is $\sigma_Q = 0.2 \frac{\mu L}{min}$. Base lengths L_0 and velocities v_0 are obtained from the acquisition at time $t = 0$ min. before switching on the PhV illumination averaging over more than 100 droplets.

$\phi = Q_d/Q_c$	$Q_c\ [\frac{\mu L}{min}]$	$Q_d\ [\frac{\mu L}{min}]$	$L_0\ [\mu m]$	$v_0\ [\mu m\ ms^{-1}]$
0.8	10	8	566 ± 7	6.29 ± 0.03
	11	8.8	566 ± 6	6.97 ± 0.04
	12.5	10	561 ± 4	8.03 ± 0.02
	15	12	563 ± 5	9.49 ± 0.07
	16.25	13	562 ± 6	10.44 ± 0.03
	17.5	14	561 ± 4	11.29 ± 0.05
	20	16	569 ± 4	13.59 ± 0.06
0.6	12	7.2	488 ± 4	7.02 ± 0.02
	16.5	9.9	476 ± 3	9.56 ± 0.03
	23.5	14.1	467 ± 7	13.65 ± 0.06
1.0	9	9	639 ± 6	6.31 ± 0.03
	13.4	13.4	638 ± 4	9.47 ± 0.04
	19	19	641 ± 4	13.6 ± 0.04

between the two phases, ε, ω, m are geometry-dependent parameters (further details in Supporting Information) and $\phi = Q_d/Q_c$. Therefore, it was possible to vary droplets length (and velocity) by properly changing the flow rates. All the used flow rates' combinations are reported in **Table 1**. Droplets base length was almost constant for fixed ϕ: in the case $\phi = 0.8$, it varied between (561 ± 4) μm and (566 ± 7) μm, for $\phi = 0.6$ it was included between (467 ± 3) μm and (488 ± 4) μm while with $\phi = 1.0$ it ranged between (638 ± 4) μm and (641 ± 4) μm. Supporting Information provides details on how the measurement of droplets lengths and velocities is performed.

Virtual electrodes had been realized by integrating an additional iron-doped lithium niobate (Fe:LN) (z-cut, 0.1 % Fe concentration) on the top of glass cover. It was well-known[14,36–38] that by illuminating Fe:LN material with suitably not-spatially homogeneous light (green, i.e., 532 nm) photoexcited electrons move in a preferential direction giving rise to a photocurrent. The latter originated in turn a charge density that results in a local space-charge electric field. The shape of the crystal region in which the field was produced depends on the shape of the illuminated spot. In the case of pure LN, the space-charge field can span from 0 to $10^4 - 10^5$ Vm^{-1}, while it was significantly increased in Fe:LN crystals, with values up to $10^6 - 10^7$ Vm^{-1} (with 0.1 % Fe concentration).[38]

The one-center charge transport model developed by Kukhtarev and coworkers[36] explained the bulk photovoltaic effect by considering only one photorefractive center, which was iron in the case of Fe:LN. In particular Fe^{2+} acted as a donor state, while Fe^{3+} as an acceptor one. This model was able to provide the time evolution of the space-charge electric field, which turns out to be an exponential law with time constant τ_{sc}:

$$E_{sc} = E_{phv}(1 - e^{-t/\tau_{sc}}) \tag{2}$$

$$\tau_{sc} = \frac{\varepsilon \varepsilon_0}{\alpha_s I} \frac{N_{Fe^{3+}}}{N_{Fe^{2+}}} = \frac{\varepsilon \varepsilon_0}{\alpha_s I} \frac{1}{R} \tag{3}$$

$$E_{phv} \propto N_{Fe^{3+}} \tag{4}$$

where $N_{Fe^{2+}}$ and $N_{Fe^{3+}}$ are respectively the density of donors and acceptors, $R = N_{Fe^{2+}}/N_{Fe^{3+}}$ is the reduction degree of the material, $\alpha_s \approx 10^{-14}$ mW^{-1} Ω^{-1} (at room temperature) is the specific photoconducivity[14] and I is the illumination intensity.

The impinging beam shape could be approximated to a circumference with $r \approx 1$ mm, hence the illumination intensity on Fe:LN could be estimated as $I = P/(\pi r^2) \approx 2.2 \cdot 10^4$ Wm^{-2}. A brief discussion on the role of laser power and wavelength in the generation of the photo-induced field could be found in Supporting Information. In this work, a z-cut Fe:LN crystal was chosen since the photoexcited electrons move along the z-axis (c-axis) toward its positive direction. Hence, the +z face was placed as close as possible to the glass cover, in order to maximize the field's lines entering the microchannel.

The scheme of the chip is reported in **Figure 2**. The illumination of the cover to promote the photovoltaic effect was provided by a solid state laser ($\lambda = 532$ nm) with a power of 65.0 mW measured in close proximity to the chip with a semiconductor power sensor connected to FieldMaxII-TO Power Meter (Coherent Inc., Santa Clara, CA, USA). In the following, this illumination would be referred to as PhV-laser (or PhV illumination) to recall its role in promoting the building up of space-charge field due to the photovoltaic effect. In parallel, a continuous diode laser with power of 7.35 mW and wavelength $\lambda = 532$ nm was coupled into the MZI waveguide, enabling the detection of the flowing droplets and the measurement of length and velocity of each single droplet.[9]

3. Results

The space-charge field has been generated by photovoltaic effect so that it interacts with moving droplets. Different droplet lengths L and velocities v were produced in trains and measured before and after the switching on of the PhV-laser, in order to investigate the effect of the space-charge field on these parameters. Each acquisition has a time duration Δt_i such that at least 100 droplets are detected for any chosen combination of flow rates and used to derive the average values of L and v. The middle point t_i of each selected Δt_i corresponds to the instant of time used to label the i−th acquisition. In **Figure 3**, an example of the behavior of the average lengths over time is reported, for the case $Q_c = 10\ \frac{\mu L}{min}$ and $Q_d = 8\ \frac{\mu L}{min}$ ($\phi = 0.8$). Experimental results show that the droplets length increases with exposition time to the PhV illumination, with a saturation value reached approximately after 30 min. The measured droplet elongation increases following an exponential law with a characteristic time of the order of magnitude of minutes, being strongly reproducible.

Up to our knowledge, no data have been published on elongations of moving droplets in microfluidic channels under photo-induced effects, such as the photovoltaic one, nor similar phenomena have been either explained or modeled. In this work, we performed systematic investigations in order to assess the role of the photo-induced field in the physical mechanisms underlying the droplet elongation. Specifically, we aim to clarify:

- The dynamics and time scale of droplet elongation phenomena and relative stability and reproducibility;
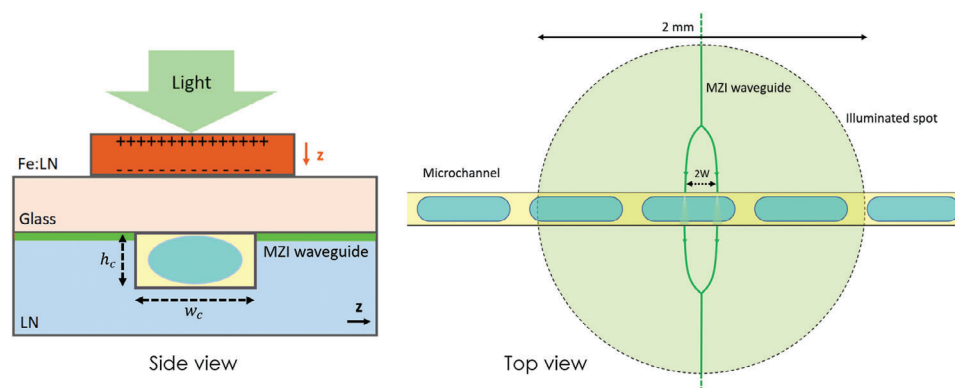
ADVANCED
SCIENCE NEWS

www.advancedsciencenews.com

ADVANCED
MATERIALS
INTERFACES
Open Access

www.advmatinterfaces.de

Figure 2. Scheme (not to scale) of the opto-microfluidic chip employed in this work. In the figure, $w_c = 200$ µm, $h_c = 100$ µm and $2W = 40$ µm. The two arrows labeled with "z" point toward the positive direction of the crystals z-axis (c-axis). The MZI waveguides were fabricated in the LN substrate prior to engraving the microchannel: the engraving process cuts perpendicularly the two arms of each waveguide in such a way that the channel is embedded in the waveguide. A detailed description of the device design and fabrication and the opto-microfluidic setup employed to generate droplets has been previously provided by our group in Ref. [9]. Device fabrication Section in Supporting Information provides the most relevant details.

- The role of the space-charge field with special care to its intensity and time scale (τ_{sc}) relative to its building-up and fading processes when the PhV illumination is switched on and off respectively;
- How the magnitude of the droplet elongation is effected by the droplet velocity, as this parameter strongly affects the duration of the interaction between E_{sc} and the droplet.

3.1. Time Scale of Droplet Elongation

If the time-dependent E_{sc} were the driven actor in modifying the droplet length, it would be expected that the main contribution of the photovoltaic effect comes from the Fe:LN sealing cover and not from the undoped LN substrate where the microfluidic channels have been engraved (a brief discussion on the contribution of the LN substrate to this phenomenon is reported in Supporting Information, Section Contribution of the LN substrate to the droplets elongation). Thus, the dopant concentration inside the

Figure 3. Average lengths over time with flow rates $Q_c = 10 \frac{\mu L}{min}$ and $Q_d = 8 \frac{\mu L}{min}$ ($\phi = 0.8$). The fit is performed with Equation (5). In this case, a Fe:LN sample with $N_{Fe^{3+}} = 15.6 \cdot 10^{18}$ atoms/cm^3 is employed.

Fe:LN sample would play a major role and the ratio R would be the key parameter to tailor the process (see Equations (2)–(3)). To assess whether this is the case, several Fe:LN sealing covers have been used in order to investigate the role of the E_{sc} intensity in the droplet elongation mechanisms. Furthermore, different dispersed phases and flow rate combinations (Table 1) have been investigated, to monitor the impact of light-induced phenomena on the droplet composition, shape, length, and velocity.

In Figure 3 results obtained using a Fe:LN top cover with $N_{Fe^{3+}} = 15.6 \cdot 10^{18}$ atoms/cm^3, $N_{Fe^{2+}} = 3.2 \cdot 10^{18}$ atoms/cm^3 and $R = 0.205 \pm 0.007$ are presented as case study since this Fe:LN sample represents the best compromise in terms of modulus and building-up time τ of the light-induced field E_{sc}. If the elongation of the droplet were induced by the photovoltaic effect, via the space-charge field generated in the Fe:LN cover, the droplet length L would scale with an exponential time dependence similar to Equation (1). In order to verify this hypothesis, experimental values of $L(t)$ have been fitted with a function:

$$L(t) = L_0 + \Delta L \left(1 - e^{-t/\tau}\right) \tag{5}$$

where L_0 is the base length when no laser beam is impinging on the iron-doped sample, while ΔL and τ are the fitting parameters. ΔL stands for the observed droplet elongation due to illumination, τ being the typical time in which that elongation is established, respectively. The proposed function well fits the experimental data of Figure 3, providing as best fitting parameters $\Delta L = 19 \pm 1$ µm and $\tau = 8 \pm 2$ min. After 60 min of illumination the PhV laser has been switched off and the values of the droplet length in absence of illumination are reported in **Figure 4**. As expected, L decreases with time, slowly approaching to the base length L_0. This is due to the fading-out transient of the space-charge field, that goes progressively to zero in absence of illumination, with a slower process than the space-charge building-up dynamics. In dark conditions, in fact, the photo-induced field decays with a typical time ranging between seconds to tens of hours,[39] depending on doping and temperature.

As it can be seen in Figure 4, a decreasing trend in the form of $L(t) = a \cdot e^{-b \cdot t} + c$ is observed with a typical lifetime ($1/b = 61$
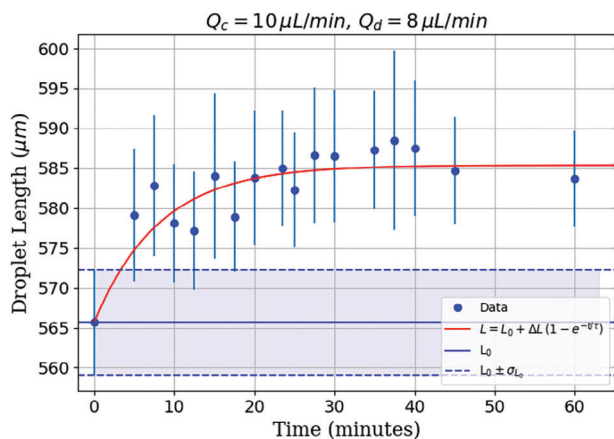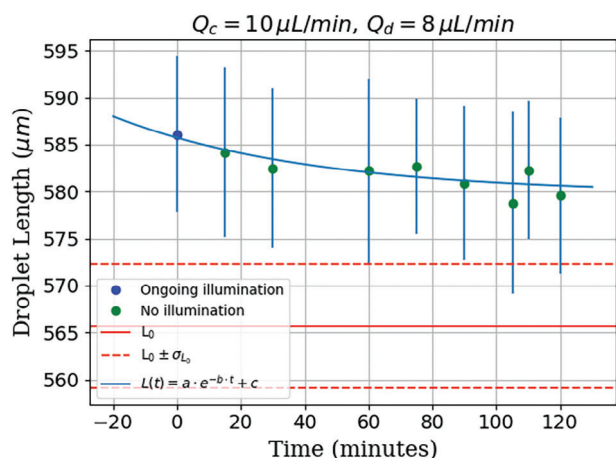
Figure 4. Average lengths over time after the switching off of the sample PhV illumination. Acquisition at t = 0 min is the one acquired at 60 min after the beginning of illumination (Figure 3). A decreasing trend is recognizable and a fitting with a chosen function in the form of is performed obtaining: $a = 6 \pm 3$ μm, $1/b = 61 \pm 1$ min and $c = 580 \pm 3$ μm. The fact that $L(t \to +\infty) = c > L_0 = 566 \pm 7$ μm suggests that the observed dynamics may be much slower than the estimation provided by the fitting parameter $1/b$.

± 1 min >8 ± 1 min). It is worth mentioning that 120 min after switching off the PhV illumination the average droplets length is still not within one standard deviation from the average length L_0.

These results clearly suggest that the droplet elongation is related to the presence of the space-charge electric field E_{sc} induced by the PhV illumination.

Since the temporal evolution of E_{sc} depends on either $N_{Fe^{3+}}$ and $N_{Fe^{2+}}$, different values of the reduction degree R = $N_{Fe^{2+}}/N_{Fe^{3+}}$ have been therefore studied, keeping fixed the dopant concentration of the Fe:LN sample ($N_{Fe} = 18.8 \cdot 10^{18} atoms/cm^3$) and the flow rates inside the microfluidic device. The employed Fe:LN samples have been characterized by means of optical absorption measurements,[40,41] obtaining the compositional parameters reported in **Table 2**. The droplet length measurements have been performed in different days, so that at least 21 h have passed between each illumination routine, allowing E_{sc} to completely fade out. Before starting each new measurement, the system has been checked to have recovered its initial state without PhV illumination, droplets' average length being compatible with the previously obtained L_0 before switching on the PhV-laser.

The fitting of the experimental data provides the parameters reported in Table 2, from which it clearly emerges a light-induced

droplet elongation of 2–3 %. These results confirm the impact of photovoltaic-induced effects on the droplet shape, since the dynamics follows Equation (5) and the phenomenon is highly reproducible. If the droplets elongation was effected only by the strength of the photo-induced field, $\Delta L/L_0$ values should follow an increasing trend (Equation (4)) and depend on $N_{Fe^{3+}}$. Data in Table 2 indeed do not confirm this expectation. Some hypothesis can then be formulated to explain this experimental evidence:

1) The investigated range of $N_{Fe^{3+}}$ is not wide enough, consequently the resolution is not high enough to highlight a dependence of L on $N_{Fe^{3+}}$;
2) It may be sufficient that $E_{sc} \geqslant E_{threshold}$ ("threshold effect") for an elongation to take place. In this specific case, the above inequality would be verified for each of the three Fe:LN samples;
3) The elongation is due to a "gradient effect", i.e., the electric field spatial variation and not its intensity plays a role in modifying the droplet length. In this case, the droplets' elongation would be caused by the dielectrophoretic force F_{dep}, which in turn depends on the spatial variation of the photo-induced electric field:

$$F_{dep} \propto \nabla |E(t)|^2 \tag{6}$$

Since the single droplet elongates only in the illuminated zone of the channel and returns to its "standard" dimension (L_0) after travelling through the electric field lines, it is expected to display a sort of spring-like behavior, which can be modeled by:

$$F_{dep} \approx k(L(t) - L_0) \approx \gamma(L(t) - L_0) \tag{7}$$

In this case, the expected dependence between the droplet length and a weakly spatially-dependent light-induced electric field would be:

$$L(t) = L_0 + \Delta L \left(1 - e^{-t/\tau}\right)^2 \tag{8}$$

In **Figure 5**, the droplets lengths are reported under different microfluidic conditions and fitted by an exponential growth and a non-linear exponential growth as discussed in Hypothesis 3). It is worth mentioning that an exponential trend seems to be compatible with the experimental data. In this work it is clear that, for all the employed samples, $E_{sc} \geqslant E_{threshold}$ holds and hypothesis 1) does not exclude 3).

In order to understand more clearly the origin of the observed exponential growth, the following aspects have been dug: i) role of the PhV exposition time, considering the illumination duration, as well as the duration of the droplet - space-charge field interaction; ii) impact of the electric field on the droplet surface tension γ; iii) impact of liquid phase polarity and screening effects.

3.2. Dynamics of Droplet Elongation

In order to understand the effect of the light exposition time on the droplet, the behavior of ΔL and τ have been studied as function of droplets velocity, namely by properly varying ϕ (Table 1). In the case of three representative velocities, L_0 has been varied
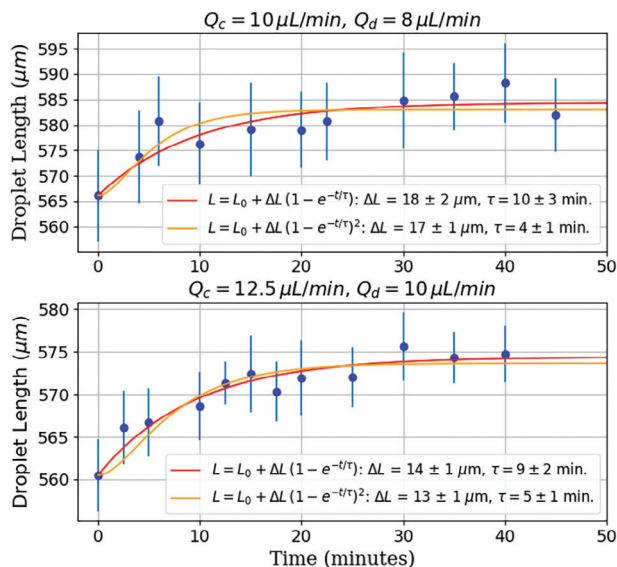
Table 2. Fit parameters of Equation (5) with flow rates $Q_c = 10 \frac{\mu L}{min}$ and $Q_d = 8 \frac{\mu L}{min}$ (ϕ = 0.8) and density of acceptors of the three employed Fe:LN samples.

R	$N_{Fe^{3+}} \left[\frac{atoms}{cm^3}\right]$	$\Delta L/L_0$ [%]	τ [min]
0.100 ± 0.006	(17.0 ± 0.3) · 10^18	3.2 ± 0.2	11 ± 3
0.205 ± 0.007	(15.6 ± 0.2) · 10^18	3.4 ± 0.2	8 ± 2
0.270 ± 0.007	(14.8 ± 0.2) · 10^18	2.3 ± 0.7	20 ± 13

**ADVANCED
SCIENCE NEWS**

www.advancedsciencenews.com

**ADVANCED
MATERIALS
INTERFACES**

www.advmatinterfaces.de

Figure 5. Average lengths over time with flow rates $Q_c = 10 \frac{\mu L}{min}$, $Q_d = 8 \frac{\mu L}{min}$ and $Q_c = 12.5 \frac{\mu L}{min}$, $Q_d = 10 \frac{\mu L}{min}$ ($\phi = 0.8$). The Fe:LN sample with $N_{Fe^{3+}} = 15.6 \cdot 10^{18}$ atoms/cm^3 is employed. The orange fits are performed with Equation (8), which is a possible candidate to capture the quadratic trend discussed in hypothesis 3 in this Section.

as well. In **Figure 6**, $\Delta L/L_0$ and τ values as a function of droplet velocity v are reported. Average droplets velocities are measured together with lengths[9] and they seem not to be affected by the photo-induced field. In fact, for each acquisition, average v_i is obtained and the values used to label each combination of flow rates in Figure 6 and **Figure 7** are the v_0 values obtained from linear fits of the kind $v = m \cdot t + v_0$, accounting in this way for all the measurements performed during illumination of the Fe:LN sample. In all cases in this work, $m \leqslant 10^{-2}$ μmms^{-2}. Droplets elongation (Figure 6) decreases with droplets velocity v in all the three ϕ values investigated. This suggests that, for the single droplet, spending more time within the illuminated zone of the channel produces more consistent elongation. Since lengths (and veloci-
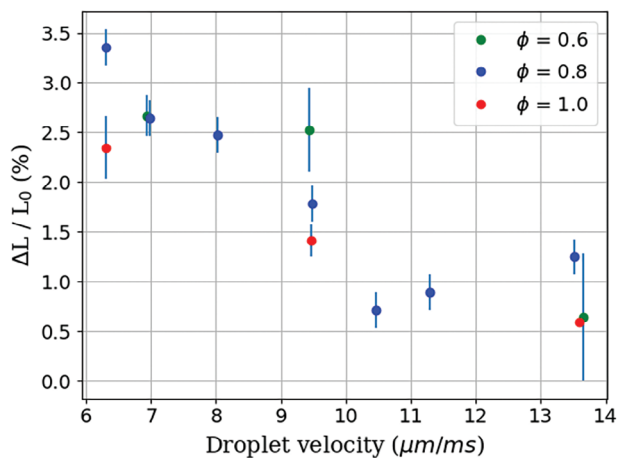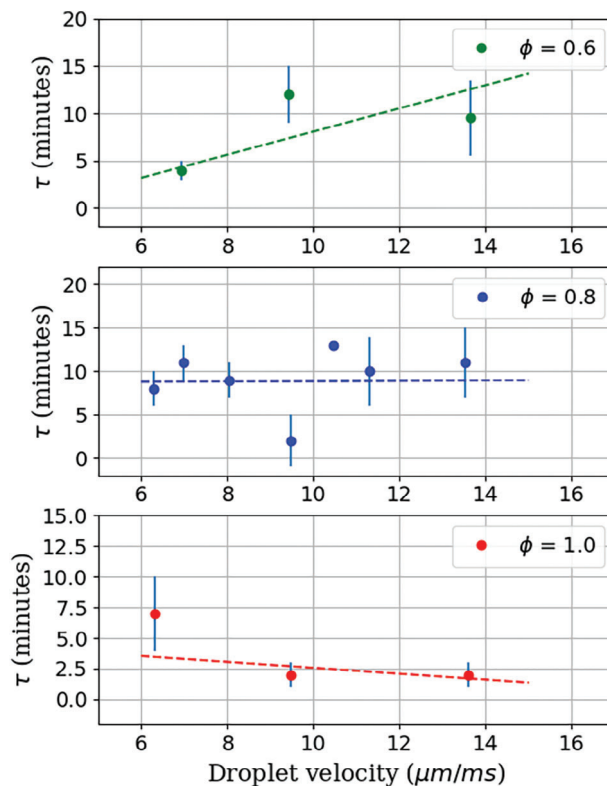

Figure 7. τ values as a function of droplet velocities fitted with a straight line equation to highlight their trend.

ties) are measured by exploiting a waveguide which is in the middle of the beam spot, two alternatives may arise: i) this acquisition setup accounts only for droplet elongation induced by illuminated zone before the waveguide and nothing can be said on the remaining part of the illuminated microchannel; ii) elongation produced while the droplet is totally within illuminated channel is negligible compared to the one induced when the droplet is entering inside the zone where the beam is impinging. The latter hypothesis implies that the gradient of the light-induced electric field $\nabla|E|$ dominates over the electric field itself in this process. As far as the τ values are concerned (Figure 7), they display different trends with v according to the corresponding ϕ value.

The faster the droplets, the higher is the required time to obtain the full elongation ΔL. This evidence is coherent with expectations, since the higher the velocity, the lower the time the photo-induced field has to interact with flowing droplets. It is also possible to notice that in the lowest velocity case, the lowest time τ is the one obtained with $\phi = 0.6$, which is consistent since this is the flow rates combination that produces smaller droplets compared to the other two. Considering that droplets' volume $V_{droplet}$ scales with their length, namely $V_{droplet} \approx L_0 w_c h_c$ with h_c the channel height, it is reasonable to assume that for the photo-induced field it is easier to interact with lower quantity of liquid. For $\phi = 0.8$ the increasing trend is however less marked, with the different values settling around $\tau = \tau_{0.8} = 8.7 \pm 0.9$ min. On the other hand, this could explain why we observe a decreasing trend for $\phi = 1.0$: the droplets' volume is too high for the field to properly

Figure 6. $\Delta L / L_0$ a function of droplet velocities. ΔL values are obtained from fits with at least 40 min of Fe:LN sample illumination.

**ADVANCED
SCIENCE NEWS**

www.advancedsciencenews.com

**ADVANCED
MATERIALS
INTERFACES**
Open Access

www.advmatinterfaces.de

interact with the fastest droplets and hence τ looses its meaning for the two higher velocity values.

Experimental data can be fitted with good agreement also with Equation (8). Resulting τ values are smaller than the one obtained in the case of Equation (5) but of the the same order of magnitude (several minutes). It is evident that the typical time τ of the observed elongation doesn't match with the photo-voltaic dynamics, namely $\tau = \tau_{sc}$ that depends only on the characteristics of the Fe:LN sample and on the illumination intensity (Equation (3)). As a matter of fact, considering $R = 0.205$, τ_{sc} is ≈ 17 s since $I \approx 2.2 \cdot 10^4$ W m^{-2} while $\varepsilon = \varepsilon_{11} = \varepsilon_{22} = 84$[14] because the chosen geometry is such that light impinging on the sample is polarized on the xy plane. As shown in Table 2, the experimental τ values are one order of magnitude bigger than τ_{sc} which means that the observed phenomenon is much slower than the building up of the photo-induced field. As a direct consequence, since at $t = 4\tau$ it must be $E(t) \approx E_{phv}$, then all the $L(t_i)$ values for $t_i > 0$ (in Figure 3) are achieved when the electric field has already reached its saturation value E_{phv}. In this case, because of Equation (7), F_{dep} should not have any temporal dependence and the same holds for the right-hand side, $\gamma \Delta L(t)$. However, since $L(t)$ follows the experimentally observed trend $L(t) \propto (1 - e^{-t/\tau})$ then γ should decrease over time as:

$$\gamma(t) \propto (1 - e^{-t/\tau})^{-1} \tag{9}$$

In order to test this hypothesis, we investigated the effect of electric field on the droplet surface tension γ.

3.3. Impact of Electric Field on the Droplet Surface Tension γ

If the droplets elongation is related to a surface tension change induced by the space-charge electric field building up, γ would depend on PhV exposition time. In order to estimate the time variation of γ over time accounting also the effect of droplets velocity, we consider the data corresponding to $\phi = 0.8$ reported in Table 1. In a T-junction, the dimensions of droplets are predicted by Equation (1), where the capillary number Ca contains viscosity of continuous phase μ_c and surface tension between the two phases, γ. Non-polar liquids viscosity is not subjected to appreciable variation in presence of electric fields up to 10^5 Vm^{-1},[42,43] hence μ_c can be considered constant during the PhV illumination. This in turn further suggests that γ plays a crucial role in this kind of dynamics. In particular, by rewriting Equation (1) as:

$$L = A(\phi)\, Ca^{-m} = A(\phi) \left(\frac{\mu\, v}{\gamma} \right)^{-m} \tag{10}$$

By using γ and μ_c values given at zero electric field, it is possible to estimate $A(\phi)$ and m when no PhV illumination is given by fixing ϕ and fitting L_0 as a function of Ca with $A(\phi)$ and m as free parameters by using Equation (10). With this approach it results that $A(\phi) = 520 \pm 20$ μm and $m = m_0 = 0.015 \pm 0.007$. Assuming that these values hold also when $E_{phv} \neq 0$, we fitted $L(t_i)$ as a function of v with Equation (10) for each set of acquisitions at different times, namely with $t_i = 5, 10, 15, 20, 25, 30, 35, 40$ min, respectively. However, this fitting procedure fails in appropriately describe the trend of $L(t_i)$ suggesting that we need

to relax the hypothesis on the parameters $A(\phi)$ and m. Hence, $L(t_i)$ has been fitted as a function of v letting the exponent m to be a fitting parameter together with γ. The fits at $t_i = 10, 20, 30$ min are reported as an example in **Figure 8a** where the experimental data trend is well reproduced. Each performed fit at $t = t_i$ yields the values $\gamma(t_i)$ and $m(t_i)$. The time behavior of $\gamma(t)$ and exponent $m(t)$ are reported in Figure 8b,c, respectively. Surface tension displays a decreasing trend over the exposition time as expected while exponent m is instead increasing with a behavior similar to the $L(t)$ time-dynamics. $\gamma(t_i)$ values are well fitted by the following function:

$$\gamma(t) = \frac{a}{\frac{1}{\gamma_0} + b(1 - e^{-t/\tau_\gamma})} = \frac{a\gamma_0}{1 + b\gamma_0(1 - e^{-t/\tau_\gamma})} \tag{11}$$

where the best parameters are $a = 1.000 \pm 0.006$, $b = (6.4 \pm 0.6) \cdot 10^3$ mN^{-1}, $\tau_\gamma = 10 \pm 2$ min. It clearly emerges that τ_γ and τ are of the same order of magnitude and the trend is compatible with predictions of Equation (5).

3.4. Screening Effects

Screening effect is expected to enter in action probing the space-charge electric field, as well as the impact of the dynamics of the droplet movement.

By keeping fixed flow rates as explained before ($Q_c = 10 \frac{\mu L}{\min}$ and $Q_d = 8 \frac{\mu L}{\min}$, $\phi = 0.8$), droplets of different NaCl solutions (NaCl dissolved in MilliQ water) dispersed in the same continuous phase are produced in this case. Dissociated Na$^+$ and Cl$^-$ ions in a NaCl solution behave as mobile charge carriers and, when exposed to an external electric field, are hence expected to position themselves in order to screen the latter. This is indeed what is observed (**Figure 9**). The average lengths' trend is clearly decreasing. The average length with zero NaCl concentration is the value obtained after 45 min of sample illumination. In the case of molar concentrations between 0.25 and 0.75 M, droplets' average lengths are compatible with L_0. This further confirms the role of the space-charge field in this observed dynamic.

3.5. Modeling

Surface tension $\gamma(t)$ is a property connected to the interface between the two phases and can depend on the presence of external electric field and on the adsorption variation of SPAN® 80 surfactant dispersed in the continuous phase. Concerning the latter, a decreasing trend of γ over time is consistent with an increased adsorption of surfactants and possibly other impurities on the water surface.[32,44–46] Conversely, accounting for the electric field increases the complexity of the system. The interaction of different kind of electric field geometries with fluids has been studied for decades starting from the pioneering work of Taylor.[47] In literature, specific geometries have been studied to describe the effect of applied electric field on interacting fluids and explain the induced deformation. Static spherical droplet or cylinder with a circular cross-section have been investigated under a uniform electric field, showing that a prolate or oblate ellipsoidal form (or ellipsoidal cross-section) is achieved according to
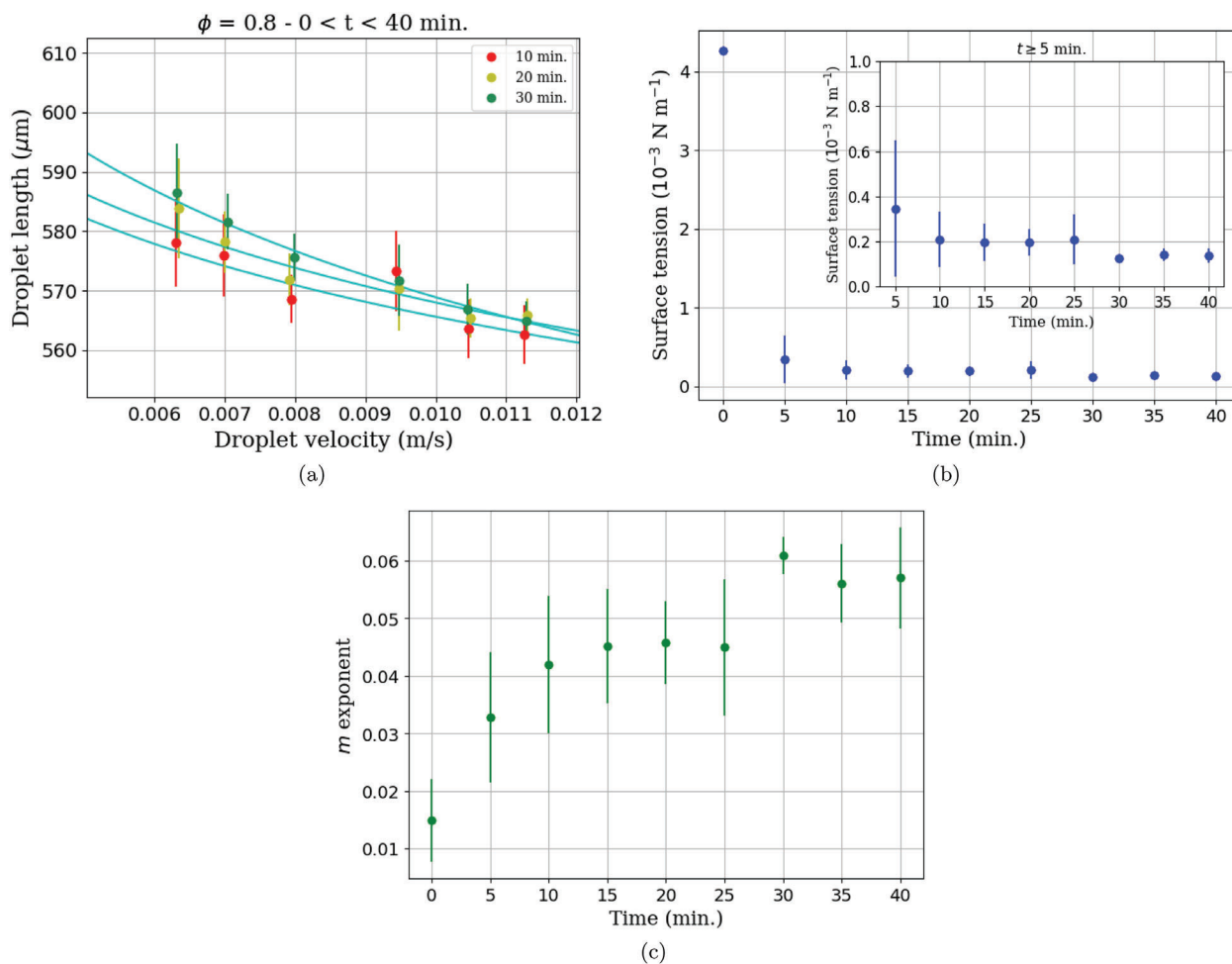
Figure 8. In Figure 8a three examples of fits of $L(t_i)$ as a function of v with Equation (10) with $t_i = 10, 20, 30$ min, by employing $A(\phi)$ parameter obtained from the fit with Equation (10) with $0.004 \leqslant Ca \leqslant 0.009$, with γ and m as fit parameters. In Figure 8b surface tension values obtained from all the fits. The point at t = 0 min. is an experimental value obtained with the pendant drop method: $\gamma_0 = 4.27 \pm 0.04$ mNm^{-1}. In Figure 8c the correspondent m values.
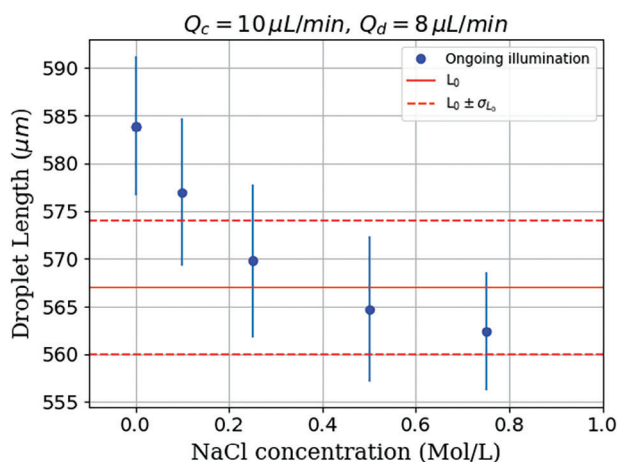
Figure 9. Trend of the obtained droplets' average lengths as a function of NaCl concentration. The average length with zero NaCl concentration is the data obtained after 45 min of sample illumination.

the electrohydrodynamic (EHD) properties of the system.[48–50] This deformation has been described basically as a process going from an initial steady state to a final one through a transient process that occurs within typical time scales of milliseconds. It is usually modeled by introducing the Taylor's deformation parameter $D = (r_\parallel - r_\perp)/(r_\parallel + r_\perp)$, with $r_\parallel$ and $r_\perp$ the droplet lengths in the directions parallel and perpendicular to the field, and solving the electrohydrodynamic problem. In our case, however, the same theoretical models cannot be used, nor a definition of D is straightforward, because the shape of the electric field lines entering the microfluidic channel and interacting with the droplets are not of a uniform electric field. Apart from having a quite complex geometry to be determined, in fact, the droplet velocity influences over time the field felt by the flowing droplets. If we considered an uniform field, within a first order approximation neglecting fluid inertia and charge relaxation,[51] for a spherical droplet the solution to the EHD problem yields:

$$D(t) = D_\infty (1 - e^{-t/\tau_d}) \tag{12}$$

$$\tau_d = \frac{\mu_c a}{\gamma} \frac{(3 + 2\kappa)(16 + 9\kappa)}{40(1 + \kappa)} \tag{13}$$

where τ_d is the characteristic time scale for the shape deformation, a the droplet radius, $\kappa = \mu_{water}/\mu_c$. In the case of a cylinder whose cross-section shifts from a circular to an ellipsoidal shape due to the interaction with a uniform transverse field the time scale τ_{co} can be obtained as:

$$\tau_{co} = \frac{(\mu_c + \mu_{water})a_c}{\gamma} \tag{14}$$

with a_c radius of the cylinder. The latter despite being a rather crude approximation compared to our case, provides an order of magnitude for the time scale of the deformation process. Inserting the values of our system in Equation (14), using $a = h_c/2 = 50$ μm, $\gamma = \gamma_0$ and $\mu_{water} = 0.89$ mPa·s at room temperature,[52] yields $\tau_{co} = 0.046$ ms, confirming that the action of the field on the deformation process is much faster and the phenomenon we are observing is a kind of interaction not yet modeled and needs to be properly understood. If we employ Equation (13), we obtain $\tau_d = 0.027$ ms, which is of the same order of magnitude but faster because of the different shape. The same order of magnitude is obtained if $a = w_c/2$ is used as approximation. The time dependence of Equation (12), which describes the transient process between steady states, suggests that the trend $L(t) \propto (1 - e^{-t/\tau})$ is expected to describe the observed phenomenon. This evidence further supports our conclusion to use Equation (5) to fit our data as motivated in the previous sections.

In this work, we assume to describe the droplet elongation in the context of relaxation processes. In this case the most simple relaxation function follows an exponential trend:[53,54]

$$\varphi(t) = \varphi_0\, e^{-t/\tau} \tag{15}$$

and it is well known that Equation (15) is a solution of the first order linear equation:

$$\frac{d\varphi(t)}{dt} = -\frac{1}{\tau}(\varphi(t) - \varphi_\infty) \tag{16}$$

with $\varphi_\infty = \varphi(t \gg \tau)$. This kind of dynamics is well reproduced by a linear oscillator that, as we have already stated, fits our droplets elongation dynamics. For a relaxation process, inertia force can be neglected[54] and the linear oscillator equation can be rewritten in the generic parameter $x(t)$ as:

$$\frac{dx(t)}{dt} + \frac{1}{\tau}x(t) = \frac{F}{k} \tag{17}$$

with τ time constant, k the spring constant and F the external harmonic force, typically time dependent. If $\varphi(t)$ solves the previous equation, also $\psi(t) = A + B\,\varphi(t)$, A, B constants, solves the same differential equation with a different final state ϕ_∞. As a consequence Equation (5) results in:

$$L(t) = L_0 + \Delta L - \Delta L\, e^{-t/\tau} \tag{18}$$
$$= L_\infty - \Delta L\, e^{-t/\tau} \tag{19}$$

i.e., a solution of a differential equation of the same kind of Equation (17). If $k \approx \gamma(t)$ (Equation (11)) with time constant $\tau_\gamma = \tau$, we can proceed with the analytical solution of the problem. Although the true expression for the force F is not known, from the trend in Figure 6 it is clear that its influence on the droplets should decrease with the velocity. Since our time scale is much slower than the deformation process, we can assume it is time independent, i.e., the following expression can be assumed:

$$F = C\left(\frac{\bar{\gamma}}{\mu_c\, \nu}\right)^\alpha \tag{20}$$

where $\alpha > 0$ and $\bar{\gamma} = \int_0^{4\tau} \gamma(t)dt/4\tau = 0.28 \cdot 10^{-3}$ Nm^{-1} to account for an average effect over time of this parameter. All the complexity of the interaction field-droplet is included within the parameter C. By assuming that ν is not significantly changing with time, Equation (17) for $L(t)$ yields:

$$L(t) = A\, e^{-t/\tau} + \frac{C}{\nu^\alpha}\frac{\bar{\gamma}^\alpha}{\mu_c^\alpha}\frac{\tau(1 + b\gamma_0)}{\gamma_0} - \frac{C}{\nu^\alpha}\frac{\bar{\gamma}^\alpha}{\mu_c^\alpha} b\, t\, e^{-t/\tau}$$
$$+ \frac{C}{\nu^\alpha}\frac{\bar{\gamma}^\alpha}{\mu_c^\alpha} B\, e^{-t/\tau} \tag{21}$$

with A and B integration constants. We can provide at this point some considerations. If $t \gg \tau$, it must be:

$$L(t \gg \tau) = L_0 + \Delta L = \frac{C}{\nu^\alpha}\frac{\bar{\gamma}^\alpha}{\mu_c^\alpha}\frac{\tau(1 + b\gamma_0)}{\gamma_0} \tag{22}$$

and as expected our final state is not time dependent. Then, when $t = 0$:

$$L(t = 0) = L_0 = A + \frac{C}{\nu^\alpha}\frac{\bar{\gamma}^\alpha}{\mu_c^\alpha}\frac{\tau(1 + b\gamma_0)}{\gamma_0} + \frac{C}{\nu^\alpha}\frac{\bar{\gamma}^\alpha}{\mu_c^\alpha} B = A + L_0 + \Delta L$$
$$+ \frac{C}{\nu^\alpha}\frac{\bar{\gamma}^\alpha}{\mu_c^\alpha} B \tag{23}$$

yielding

$$A + \frac{C}{\nu^\alpha}\frac{\bar{\gamma}^\alpha}{\mu_c^\alpha} B = -\Delta L \tag{24}$$

and Equation (21) takes the following form:

$$L(t) = L_0 + \Delta L(1 - e^{-t/\tau}) - \frac{C}{\nu^\alpha}\frac{\bar{\gamma}^\alpha}{\mu_c^\alpha} b\, t\, e^{-t/\tau} \tag{25}$$

Interestingly, we were able to recover the same shape of Equation (5) except for a correction containing the parameters C and b, both describing the interaction between the electric field and the flowing droplets. We note that this additional term does not affect the final length reached by the droplets as it vanishes when $t \gg \tau$. Since experimentally we do not observe such correction scaling with $t\, e^{-t/\tau}$ we expect the parameter C to be sufficiently small. We can fit the data corresponding to $\phi = 0.8$ in Figure 6 with the following equation, which is a rewritten form
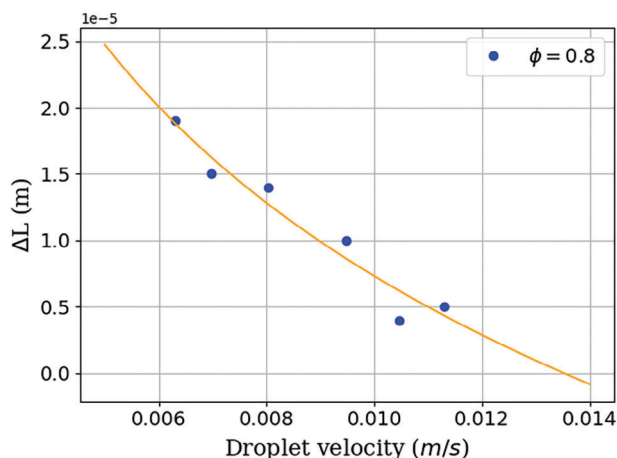
**ADVANCED
SCIENCE NEWS**

www.advancedsciencenews.com

**ADVANCED
MATERIALS
INTERFACES**

www.advmatinterfaces.de

Figure 10. Experimental values of ΔL values ($\phi = 0.8$) as a function of droplet velocity. The yellow line represents the fit of the data using Equation (26).

of Equation (22), to obtain an estimation of C and α exponent:

$$\Delta L = \frac{C}{v^\alpha} \frac{\bar{\gamma}^\alpha}{\mu_c^\alpha} \frac{\tau(1 + b\gamma_0)}{\gamma_0} - L_0 =$$

$$= \frac{C}{v^\alpha} \left(\frac{\bar{\gamma}}{\mu_c}\right)^\alpha \frac{\tau(1 + b\gamma_0)}{\gamma_0} - A(\phi) \left(\frac{\gamma_0}{\mu_c}\right)^{m_0} \frac{1}{v^{m_0}} \quad (26)$$

where we used Equation (10) and $\tau = \tau_{0.8} = 8.7$ min. Fitting procedure provides a good agreement with our data (**Figure 10**) yielding $C = (1.45 \pm 0.02) \cdot 10^{-10}$ N s^{-1} and $\alpha = 0.058 \pm 0.006$. The parameter C is in fact small, yet the additional factor provides a trend which is not observed experimentally (**Figure 11**). This is in perfect agreement with our model since no constrains have been included by the microfluidic channel. As a consequence, the droplet can elongate appreciably only in the direction of its motion, while in the two perpendicular direction the channel's walls opposes to the deformation (Supporting Information Section Droplet deformation in the directions perpendicular to
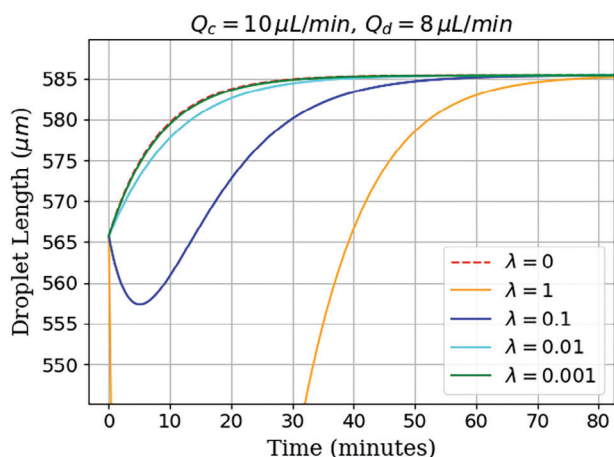

Figure 11. Comparison of different λ values inserted in Equation (27) with ΔL and τ corresponding to the data in Figure 3. The curve with $\lambda = 0$ corresponds to the fitted Equation (5).

the main channel provides an estimation on the deformation on the directions perpendicular to the droplets motion). Such constraint is quite difficult to be imposed since we cannot directly measure the deformation of the cross-section. Empirically we could account for this by adding a phenomenological parameter λ to the term proportional to t in Equation (25), so that:

$$L(t) = L_0 + \Delta L(1 - e^{-t/\tau}) - \lambda \frac{C}{v^\alpha} \frac{\bar{\gamma}^\alpha}{\mu_c^\alpha} b t e^{-t/\tau} \quad (27)$$

where $\lambda = 10^{-2}$ matches with our observed trend given by Equation (5) (Figure 11).

Finally, rewriting Equation (26) to obtain τ yields:

$$\tau = \frac{\gamma_0}{C(1 + b\gamma_0)} \left(\frac{\mu_c}{\bar{\gamma}}\right)^\alpha (L_0 + \Delta L) v^\alpha \quad (28)$$

which means that a dependence of τ on v cannot be ruled out. The varying trend with varying ϕ (Figure 7) suggests that α exponent and C may be dependent on ϕ as well.

4. Conclusion

In this work, we have investigated the dynamics of a photo-induced electric field by studying its action on water droplets flowing in a continuous phase (Hexadecane) inside an opto-microfluidic platform integrated on a LN substrate. The dynamics of the photo-induced field was investigated by studying its action on dispersed phase's droplets flowing in a continuous phase (Hexadecane), immiscible with the dispersed one (water), generated by exploiting an opto-microfluidic platform integrated on a LN substrate. Droplets generation was achieved thanks to the integrated microfluidic stage, consisting of a cross-junction engraved in the LN substrate, while droplets detection during their motion across the main microchannel was achieved by exploiting the optical stage of the device, namely an array of Ti-indiffused optical waveguides in Mach-Zehnder interferometer (MZI) configuration perpendicular to the microchannel. The electric field was obtained by suitably illuminating with a green laser beam a Fe:LN sample, integrated in the same device, so that the impinging light was in correspondence of the MZI waveguide. To the knowledge of the authors, this is the first time that the dynamics of the Fe:LN photo-induced field is investigated by directly observing its effect on dispersed droplets generated and detected thanks to an opto-microfluidic platform in such a configuration. Droplets of three similar lengths and different velocities were generated by suitably varying flow rates of continuous and dispersed phase to investigate photo-induced field effects on droplets of different size and velocity. An increasing of droplets' average lengths over time during illumination of Fe:LN sample is observed in all the cases, with a stabilization around a constant value after a typical time τ. Although it is not clear up to now which is the best function describing the behavior of the average lengths over time during illumination, such a trend is reasonably compatible with the dynamics of the photo-induced space-charge electric field. The elongation effect is observed when employing three Fe:LN samples with different doping, which is again consistent with theoretical models available in the literature, being the photo-induced field dynamics dependent on the Fe doping level

of the crystal. Droplet elongation ΔL due to the light-induced field and typical building-up time τ were investigated as a function of droplets velocity (and base length L_0), highlighting a decreasing trend of ΔL with velocity and a dependence of τ on droplets size. If dispersed phase is varied by adding NaCl, a screening effect is observed with increasing NaCl concentration. Our model is nevertheless able to reproduce quite well the trend of the observed elongation ΔL. Our choices for the functional form of $\gamma(t)$ and F were a justified attempt to gather the essential physics involved in the observed dynamics.

The simplicity and the flexibility ensured by the opto-microfluidic platform presented here and these promising results pave the way for future improvements and studies, opening new interesting possibilities, e.g., manipulating dispersed objects within droplets by tuning doping level of Fe:LN and/or suitably varying flow rates, modifying droplets size and velocity, and dispersed phase properties.

Supporting Information

Acknowledgements

Conflict of Interest

The authors declare no conflict of interest.

Data Availability Statement

The data that support the findings of this study are available from the corresponding author upon reasonable request.

Keywords

[1] S. Haeberle, R. Zengerle, *Lab Chip* **2007**, *7*, 1094.
[2] D. Mark, S. Haeberle, G. Roth, F. V. Stetten, R. Zengerle *NATO Science for Peace and Security Series A: Chemistry and Biology*, Springer Netherlands **2010**, pp. 305–376.
[3] G. Bettella, R. Zamboni, G. Pozza, A. Zaltron, C. Montevecchi, M. Pierno, G. Mistura, C. Sada, L. Gauthier-Manuel, M. Chauvet, *Sens. Actuators, B* **2019**, *282*, 391.
[4] L. Zanini, A. Zaltron, E. Turato, R. Zamboni, C. Sada, *Sensors* **2022**, *22*, 1144.
[5] A. C. Bedoya, C. Monat, P. Domachuk, C. Grillet, B. J. Eggleton, *Appl. Opt.* **2011**, *50*, 2408.
[6] R. Zamboni, A. Zaltron, E. Izzo, G. Bottaro, D. Ferraro, C. Sada, *Sensors* **2020**, *20*, 5366.
[7] J. Kim, J. Erath, A. Rodriguez, C. Yang, *Lab Chip* **2014**, *14*, 2480.
[8] C.-G. Yang, Z.-R. Xu, J.-H. Wang, *TrAC, Trends Anal. Chem.* **2010**, *29*, 141.
[9] R. Zamboni, A. Zaltron, M. Chauvet, C. Sada, *Sci. Rep.* **2021**, *11*, 1.
[10] Y. Ding, P. Howes, A. deMello, *Analyt. Chem.* **2019**, *92*, 132.
[11] J. Hartmann, M. Schür, S. Hardt, *Nat. Commun.* **2022**, *13*, 1.
[12] A. Zaltron, D. Ferraro, A. Meggiolaro, S. Cremaschini, M. Carneri, E. Chiarello, P. Sartori, M. Pierno, C. Sada, G. Mistura, *Adv. Mater. Interfaces* **2022**, *9*, 22.
[13] D. R. Link, E. Grasland-Mongrain, A. Duri, F. Sarrazin, Z. Cheng, G. Cristobal, M. Marquez, D. A. Weitz, *Angew. Chem., Int. Ed.* **2006**, *45*, 2556.
[14] T. Volk, M. Wöhlecke, *Lithium niobate: defects, photorefraction and ferroelectric switching*, vol. 115, Springer Science & Business Media, Berlin, Heidelberg **2008**.
[15] V. Fridkin, *Crystallogr. Rep.* **2001**, *46*, 654.
[16] A. Zaltron, G. Bettella, G. Pozza, R. Zamboni, M. Ciampolillo, N. Argiolas, C. Sada, S. Kroesen, M. Esseling, C. Denz, in *SPIE Proceedings*, (Eds.: F. Baldini, J. Homola, R. A. Lieberman), SPIE, Bellingham, WA **2015**.
[17] G. Bettella, G. Pozza, S. Kroesen, R. Zamboni, E. Baggio, C. Montevecchi, A. Zaltron, L. Gauthier-Manuel, G. Mistura, C. Furlan, M. Chauvet, C. Denz, C. Sada, *Micromachines* **2017**, *8*, 185.
[18] A. Quelennec, J. J. Gorman, D. R. Reyes, *Nat. Commun.* **2022**, *13*, 1.
[19] S. Bonfadini, F. Ciciulla, L. Criante, A. Zaltron, F. Simoni, V. Reshetnyak, L. Lucchetti, *Sci. Rep.* **2019**, *9*, 1.
[20] R. D. Janardhana, N. Jackson, *Sensors* **2023**, *23*, 8317.
[21] X. Qin, X. Chen, L. Li, H. Wang, X. Wei, *Sens. Actuators A: Phys.* **2022**, *341*, 113568.
[22] D. Nwatu, D. Kip, K. Hasse, *Opt. Express* **2023**, *31*, 37618.
[23] X. Zhao, Z. Chen, Y. Qiu, N. Hao, *Mater. Adv.* **2023**, *4*, 988.
[24] R. Zamboni, L. Gauthier-Manuel, A. Zaltron, L. Lucchetti, M. Chauvet, C. Sada, *Opt. Express* **2023**, *31*, 28423.
[25] V. Marchesano, O. Gennari, L. Mecozzi, S. Grilli, P. Ferraro, *ACS Appl. Mater. Interfaces* **2015**, *7*, 18113.
[26] A. Chiasera, Y. Dumeige, P. Feron, M. Ferrari, Y. Jestin, G. Nunzi Conti, S. Pelli, S. Soria, G. C. Righini, *Laser Photonics Rev.* **2010**, *4*, 457.
[27] L. He, Ş. K. Özdemir, L. Yang, *Laser Photonics Rev.* **2013**, *7*, 60.
[28] S. Avino, A. Krause, R. Zullo, A. Giorgini, P. Malara, P. De Natale, H. P. Loock, G. Gagliardi, *Adv. Opt. Mater.* **2014**, *2*, 1155.
[29] N. Toropov, G. Cabello, M. P. Serrano, R. R. Gutha, M. Rafti, F. Vollmer, *Light: Sci. Appl.* **2021**, *10*, 42.
[30] V. D. Ta, R. Chen, H. D. Sun, *Sci. Rep.* **2013**, *3*, 1362.
[31] Z. Liu, L. Liu, Z. Zhu, Y. Zhang, Y. Wei, X. Zhang, E. Zhao, Y. Zhang, J. Yang, L. Yuan, *Opt. Lett.* **2016**, *41*, 4649.
[32] G. Pirnat, M. Humar, *Adv. Photonics Res.* **2021**, *2*, 2100129.
[33] P. Garstecki, M. J. Fuerstman, H. A. Stone, G. M. Whitesides, *Lab Chip* **2006**, *6*, 437.
[34] G. F. Christopher, N. N. Noharuddin, J. A. Taylor, S. L. Anna, *Phys. Rev. E* **2008**, *78*, 3.

[35] H. Liu, Y. Zhang, *Phys. Fluids* **2011**, *23*, 8.

[36] N. V. Kukhtarev, V. B. Markov, S. G. Odulov, M. S. Soskin, V. L. Vinetskii, *Ferroelectrics* **1978**, *22*, 949.

[37] P. Günter, J. Huignard, *Photorefractive materials and their applications*, vol. *114*, Springer, Germany **2007**.

[38] L. Lucchetti, K. Kushnir, A. Zaltron, F. Simoni, *J. European Opt. Soc. - Rapid Publications* **2016**, *11*, 16007.

[39] D. Kip, J. Hukriede, E. Krätzig, *Phys. Status Sol. A Appl. Res.* **1998**, *168*, R3.

[40] M. V. Ciampolillo, A. Zaltron, M. Bazzan, N. Argiolas, C. Sada, *Appl. Spectrosc.* **2011**, *65*, 216.

[41] F. Ciciulla, A. Zaltron, R. Zamboni, C. Sada, F. Simoni, V. Y. Reshetnyak, L. Lucchetti, *Crystals* **2021**, *11*, 908.

[42] E. Alcock, *Physics* **1936**, *7*, 126.

[43] E. Andrade, N. D. Costa, C. Dodd, *Proc. R. Soc. A: Math. Phys. Sci.* **1946**, *187*, 296.

[44] G. Berg, L. E. Lundgaard, N. Abi-Chebel, *Chem. Eng. Process.* **2010**, *49*, 1229.

[45] J. R. Campanelli, X. Wang, *J. Colloid Interface Sci.* **1999**, *213*, 340.

[46] W. Wang, Z. Zhou, K. Nandakumar, Z. Xu, J. H. Masliyah, *J. Colloid Interface Sci.* **2004**, *274*, 625.

[47] G. I. Taylor, *Proc. R. Soc. A: Math. Phys. Sci.* **1966**, *291*, 159.

[48] S. Moriya, K. Adachi, T. Kotaka, *Langmuir* **1986**, *2*, 155.

[49] A. Esmaeeli, P. Sharifi, *Phys. Rev. E* **2011**, *84*, 036308.

[50] J. A. Lanauze, L. M. Walker, A. S. Khair, *Phys. Fluids* **2013**, *25*, 112101.

[51] F. Ciciulla, A. Zaltron, R. Zamboni, C. Sada, F. Simoni, V. Y. Reshetnyak, L. Lucchetti, *Crystals* **2021**, *11*, 908.

[52] W. Haynes, D. Lide, T. Bruno, *CRC handbook of chemistry and physics*, CRC Press, Boca Raton, FL **2016**.

[53] K. L. Ngai, *Relaxation and diffusion in complex systems*, Springer Science & Business Media, Berlin, Heidelberg **2011**.

[54] A. Lukichev, *Phys. Lett. A* **2019**, *383*, 2983.